The FEBS Journal

FEBS PRESS science publishing by scientists

Farnesylation of human guanylate-binding protein 1 as safety mechanism preventing structural rearrangements and uninduced dimerization

Charlotte Lorenz[1,2], Semra Ince[3], Tao Zhang[4], Anneliese Cousin[5], Renu Batra-Safferling[5], Luitgard Nagel-Steger[4], Christian Herrmann[3] and Andreas M. Stadler[1,2]

1 Jülich Centre for Neutron Science (JCNS-1) and Institute for Complex Systems (ICS-1), Forschungszentrum Jülich GmbH, Germany
2 Institute of Physical Chemistry, RWTH Aachen University, Germany
3 Physical Chemistry I, Faculty of Chemistry and Biochemistry, Ruhr-University, Bochum, Germany
4 Institut für Physikalische Biologie, Heinrich-Heine-Universität Düsseldorf, Germany
5 Institute of Complex Systems (ICS-6), Structural Biochemistry, Forschungszentrum Jülich GmbH, Germany

Keywords
AUC; dimerization; farnesylation; GTPase; integrative structural modelling; SAXS

Correspondence
A. M. Stadler, Jülich Centre for Neutron Science (JCNS-1) and Institute for Complex Systems (ICS-1), Forschungszentrum Jülich GmbH, 52425 Jülich, Germany
E-mail: a.stadler@fz-juelich.de

(Received 3 December 2018, revised 25 June 2019, accepted 19 July 2019)

doi:10.1111/febs.15015

Human guanylate-binding protein 1 (hGBP1) belongs to the family of dynamin-like proteins and is activated by addition of nucleotides, leading to protein oligomerization and stimulated GTPase activity. *In vivo*, hGBP1 is post-translationally modified by attachment of a farnesyl group yielding farn-hGBP1. In this study, hydrodynamic differences in farn-hGBP1 and unmodified hGBP1 were investigated using dynamic light scattering (DLS), analytical ultracentrifugation (AUC) and analytical size-exclusion chromatography (SEC). In addition, we performed small-angle X-ray scattering (SAXS) experiments coupled with a SEC setup (SEC-SAXS) to investigate structural properties of nonmodified hGBP1 and farn-hGBP1 in solution. SEC-SAXS measurements revealed that farnesylation keeps hGBP1 in its inactive monomeric and crystal-like conformation in nucleotide-free solution, whereas unmodified hGBP1 forms a monomer–dimer equilibrium both in the inactive ground state in nucleotide-free solution as well as in the activated state that is trapped by addition of the nonhydrolysable GTP analogue GppNHp. Nonmodified hGBP1 is structurally perturbed as compared to farn-hGBP. In particular, GppNHp binding leads to large structural rearrangements and higher conformational flexibility of the monomer and the dimer. Structural changes observed in the nonmodified protein are prerequisites for further oligomer assemblies of farn-hGBP1 that occur in the presence of nucleotides.

Database
All SEC-SAXS data, corresponding fits to the data and structural models are deposited in the Small Angle Scattering Biological Data Bank [SASBDB (*Nucleic Acids Res*, 43, 2015, D357)] with project IDs: SASDEE8, SASDEF8, SASDEG8, SASDEH8, SASDEJ8, SASDEK8, SASDEL8 and SASDEM8.

Abbreviations
AUC, analytical ultracentrifugation; DLS, dynamic light scattering; farn-hGBP1, farnesylated hGBP1; G protein, GTP-binding protein; GADs, G proteins that are activated by nucleotide-dependent dimerization; hGBP1, human guanylate-binding protein 1; HIC, hydrophobic interaction chromatography; LG, large GTPase domain; MW, molecular weight; R_g, Radius of gyration; R_h, Stokes radius or hydrodynamic radius; SAXS, small-angle X-ray scattering; SEC-SAXS, size-exclusion chromatography coupled with small-angle X-ray scattering; SEC, size-exclusion chromatography; V_e, elution volume; V_o, void volume.

Introduction

GTP-binding proteins are found in all three kingdoms of life and are mainly involved in regulatory functions of cellular processes like membrane deformation and signal transduction [1]. According to Gasper *et al.* [2], GTP-binding proteins can further be divided into conventional G proteins like Ras proteins with high nucleotide affinity and the necessity for nucleotide exchange factors for activation and signalling, and into G proteins that are activated by nucleotide-dependent dimerization (GADs). GADs are structurally characterized by the presence of large GTPase domains, a low intrinsic nucleotide affinity and cooperative GTPase activity upon self-assembly [2]. Furthermore, many members of this family are able to interact with lipid membranes [3]. Dynamin is a prominent member of the GAD family, which upon GTP binding and hydrolysis is able to catalyse scission of vesicles [4] from membranes by forming long helical oligomers [5].

Human guanylate-binding protein 1 (hGBP1) belongs to the family of dynamin-related large GTP-binding proteins [6]. The crystal structure of full-length hGBP1 consists of three domains (Fig. 1A), a N-terminal large GTPase domain (LG), a middle domain consisting of α-helices and a GTPase effector domain. Overall, the crystal structure (Fig. 1A) is elongated with the globular N-terminal LG domain on one side and a long α-helix 12 spanning back from the middle domain to the LG domain over a range of approximately 130 Å. This helix is followed by the very short α-helix 13, which runs antiparallel and closely packed to α-helix 12. The three members hGBP1, hGBP2 and hGBP5 of the hGBP family possess a C-terminal prenylation motif (CaaX) that leads to post-translational attachment of a C-15 or C-20 isoprenyl group [7]. In the case of hGBP1, it was shown that the C-15 farnesyl moiety is covalently attached to the cysteine of the CaaX-binding motif (Fig. 1A). This modification is essential for intracellular formation of vesicle-like structures [7]. Moreover, it was shown *in vitro* that vesicle association is dependent on farnesylation [8].

Oligomerization properties of hGBP1 after nucleotide addition were reported first from size-exclusion chromatography (SEC) and dynamic light scattering (DLS) experiments. Without nucleotides, hGBP1 was proposed to be monomeric, whereas after addition of nonhydrolyzable GTP analogues like GppNHp, it was classified as a dimer [6,9]. Dimerization of hGBP1 is most prominently mediated by the formation of head-to-head dimers that are facing each other via the LG domain interfaces, as it was suggested from crystal structures of the isolated LG domains in the presence of nucleotides and other biochemical assays like mutational studies [9,10]. A potential hGBP1 dimer model based on the crystallographic LG domains and the monomer crystal structure is shown in Fig. 1B. More recently, in a study by Vöpel *et al.* [11] based on FRET and EPR distance measurements, the crystal dimer model has been challenged. It has been suggested that in addition to the crystallographic dimer model there exists a distorted and more opened hGBP1 dimer in solution as well. In the opened hGBP1 dimer, helices 13 can interact with each other forming a coiled-coil structure, which is not possible in the crystallographic dimer model due to structural constraints. Moreover, interaction of helices 13 in the dimer would allow to bring the farnesyl groups of two proteins in close contact as the farnesyl group is attached to the C-terminal CaaX motif of helix 13. In the first description of farn-hGBP1 purification by Fres *et al.* [8], it was proposed that hGBP1 undergoes structural changes after farnesylation as the protein surface is less hydrophobic compared to the nonfarnesylated protein, which was observed during purification on a hydrophobic interaction chromatography column [8]. It was proposed that the C terminus with its hydrophobic amino acids is internally hidden after farnesylation [8].

In this study, we investigated the structural differences between the ground states (inactive/nucleotide free) of the unmodified and farnesylated hGBP1 (farn-hGBP1) in solution. In addition, we investigated the effect of GppNHp binding on unmodified hGBP1. GppNHp is a nonhydrolyzable analogue mimicking the nucleotide-bound state in solution. For that purpose, we have performed a set of experiments using DLS, SEC and analytical ultracentrifugation (AUC). After observation of differences in their hydrodynamic properties, we have used small-angle X-ray scattering (SAXS) to clarify the structural origin of the hydrodynamic differences. We found a monomer–dimer equilibrium with a dimer fraction of around 10–20% of the commonly used nonmodified hGBP1 even in nucleotide-free solution and in the presence of GppNHp under standard conditions (2 $mg{\cdot}mL^{-1}$ or 30 μM hGBP1 in Tris buffered solution at pH 7.9). Moreover, we observed strong structural perturbations of the hGBP1 monomer in the presence of GppNHp. The hGBP1 dimer was found to be structurally distorted and the obtained solution structures agree with an opened solution structure, which might be relevant for oligomerization of farn-hGBP1 as described in recent electron microscopy and fluorescence studies [12]. The combination of the different techniques led

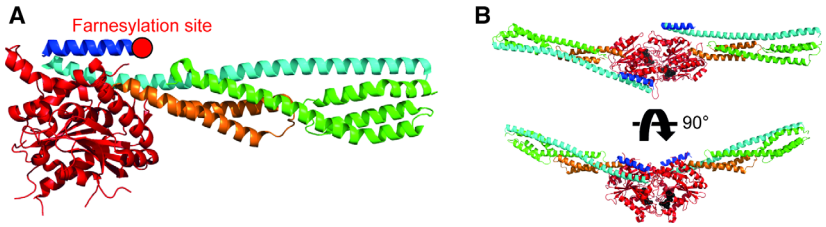

Fig. 1. Crystal structure of hGBP1. (A) Domain structure of hGBP1 monomer (pdb ID 1DG3). The C-terminal farnesylation site is marked with a red circle. LG domain in red, Middle Domain in orange and green, α-helical domains 12 and 13 in cyan and blue. (B) Dimer model created from alignment of two monomeric full-length protein crystal structures in the presence of GppNHp (pdb ID 1F5N) with crystallized LG domain dimers in the presence of GppNHp (pdb ID 2BC9).

us to the conclusion that farnesylation of hGBP1 is needed to prevent oligomerization and to stabilize the inactive ground state before activation of hGBP1 by nucleotides in solution occurs ensuring a controlled signal transduction mechanism.

Results

Verification of monodispersity and quality control by DLS

Dynamic light scattering was measured to verify the required sample quality for AUC and SAXS experiments and to determine the hydrodynamic radius R_h of the protein at infinite dilution. Nucleotide-free solutions of hGBP1 and farn-hGBP1 as well as hGBP1 solution containing 1 mM GppNHp were measured using DLS. Intensity-weighted size distributions of all investigated samples show only one peak demonstrating the absence of protein aggregation at all measured protein concentrations. Illustratively, the fitted time correlation data and intensity-weighted size distributions obtained from 1 mg·mL^{-1} protein solutions are shown in Fig. 2. Hydrodynamic radii were calculated from the DLS correlation functions and the R_h values were linearly extrapolated for $c \rightarrow 0$ mg·mL^{-1}. R_h values at infinite dilution of the investigated samples are given in Table 1. Theoretical R_h values were calculated from the monomer crystal structure (1DG3) and the dimer model (1F5N – 2BC9) using the computer programs HYDROPRO and SOMO, see Table 1.

The calculated R_h values of the monomer crystal structure are 4.0/3.8 nm (HYDROPRO/SoMo) and 5.7/5.3 nm for the dimer model. All experimentally determined diffusion coefficients lie between the theoretical values of monomer and dimer. The measured hydrodynamic radius of farn-hGBP1 with 4.74 nm is smaller than that of nucleotide-free hGBP1 with 5.73 nm, although hGBP1 in nucleotide-free solution was proposed to be monomeric. As described earlier [13], we observe an increase in the measured R_h value of hGBP1 upon addition of GppNHp. That observation would be in agreement with assumed dimerization of hGBP1 in the presence of GppNHp [13].

Our DLS experiments point out that farn-hGBP1 has similar hydrodynamic properties compared to the crystal structure of hGBP1, whereas hGBP1 in nucleotide-free solution and in the presence of GppNHp has a larger apparent hydrodynamic radius lying in between that of the theoretical values of monomer and dimer. DLS does not allow to separate an eventually occurring monomer–dimer equilibrium. A mixture of monomer and dimer would result in a higher apparent hydrodynamic radius. A structural expansion of monomeric hGBP1 would also result in a larger hydrodynamic radius possibly approaching that of the hGBP1 dimer model. Therefore, the larger hydrodynamic radii of hGBP1 in nucleotide-free and in the presence of GppNHp could be either caused by a monomer–dimer equilibrium or due to structural expansion of monomeric hGBP1. Hence, we investigated the oligomeric distribution further using SEC and AUC experiments that allow to distinguish monomers and dimers in solution.

Hydrodynamic properties investigated by SEC and AUC

Size-exclusion chromatography experiments of hGBP1 were already performed in earlier studies [6,14,15] with the aim to determine the oligomeric state of hGBP1 in solution. An important recent finding was that the elution properties of hGBP1 are not only dependent on the presence or absence of nucleotides but also on the salt concentration. Therefore, we ensured that the chosen buffer composition in our study is the same buffer condition as described in the previous work [15]. Molecular mass calibration of SEC columns is routinely performed for globular proteins, which obey a linear correlation of $R_h^3 \propto M_m$. For the case of

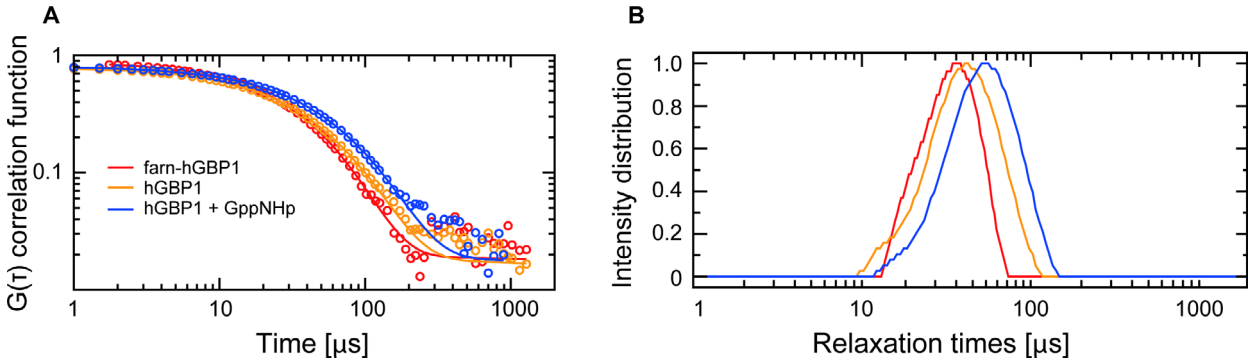

Fig. 2. Dynamic light scattering of farn-hGBP1, hGBP1 and hGBP1 in the presence of GppNHp (red: farn-hGBP1, orange: hGBP1, blue: hGBP1 + 1 mM GppNHp). (A) Exemplary time correlation data of one DLS measurement and fit of 1 mg·mL^{-1} hGBP1. Raw auto correlation data are shown as dots and regularization fits performed by the ZETASIZER software as lines. (B) Intensity-weighted size distribution function versus relaxation times for all three conditions obtained from the Zetasizer analysis shown in panel (A).

Table 1. Hydrodynamic radii from calculations and DLS experiments.

	DLS R_h [nm]	R_h [nm] HYDROPRO	R_h [nm] SoMo
Monomer (1DG3)		4.0	3.8
farn-hGBP1	4.74 ± 0.04		
hGBP1	5.73 ± 0.12		
hGBP1 + GppNHp	6.02 ± 0.13		
Dimer (1F5N – 2BC9)		5.7	5.3

hGBP1 that correlation between R_h and M_m is not maintained, as the monomeric crystal structure is already very elongated. This becomes obvious when comparing the obtained molecular masses of the monomeric elution fractions, which would be 72.83 kDa for farn-hGBP1, 85.83 kDa for hGBP1 and 103.01 kDa for GppNHp, whereas the theoretical molecular weight of a monomer would be 69.17 kDa. The discrepancy is more pronounced for the second elution peak of the dimer fraction. There we obtain molecular masses of 236.40 kDa for hGBP1 and 274.72 kDa in the presence of GppNHp, which is in the range of trimers to tetramers. The dimeric nature of this second species is corroborated from the following AUC experiments and will further be discussed from the SEC-SAXS results where scattering intensity and concentration measurement in-line can confirm the dimeric nature of this eluting species. This information leads to the conclusion that for hGBP1, the standard molecular weight calibration of SEC elution volumes is not suitable.

Therefore, we performed a calibration of the SEC column based on the hydrodynamic radius of reference proteins calculated using the program SOMO as described in the section Materials and Methods in detail. Obtained SEC elution profiles of hGBP1 and farn-hGBP1 in nucleotide-free solution as well as of hGBP1 in the presence of GppNHp are shown in Fig. 3B. The molecular masses, Stokes radii and volume fractions obtained from SEC experiments and theoretical R_h values of the monomer (pdb ID 1DG3) and dimer model (1F5N-2BC9) calculated with SoMo are summarized in Table 2. The separation based on hydrodynamic properties on the SEC column in nucleotide-free solution shows pronounced differences between farnesylated and unmodified hGBP1 similar to the previous DLS results. Whereas farn-hGBP1 elutes as one peak from the column with a hydrodynamic radius of 3.77 nm, two elution peaks with R_h values of 3.82 and 5.01 nm for nucleotide-free hGBP1 are visible. In the presence of GppNHp, hGBP1 shows a similar elution profile compared to nucleotide-free condition with the monomer as the main elution fraction and the dimer giving a secondary peak corresponding to shifted R_h values of 4.01 and 5.22 nm respectively. Apparently, the SEC column used in our study shows a higher separation capacity than that used in a previous study [15], where SEC peaks due to hGBP1 dimers only appeared as broad shoulders. The lower separation capacity of the column used by Ince *et al.* [15] is most likely due to ageing of the column (personal communication).

The SEC results affirm the initial observation by DLS that farn-hGBP1 appears always monodisperse in the most compact conformation corresponding to a pure monomer fraction. Moreover, the hydrodynamic radius of 3.77 nm is in excellent agreement with the theoretical R_h of the crystal structure conformation of the monomeric hGBP1 (R_h = 3.79 nm calculated with SoMo of pdb ID 1DG3). Without the farnesylation,

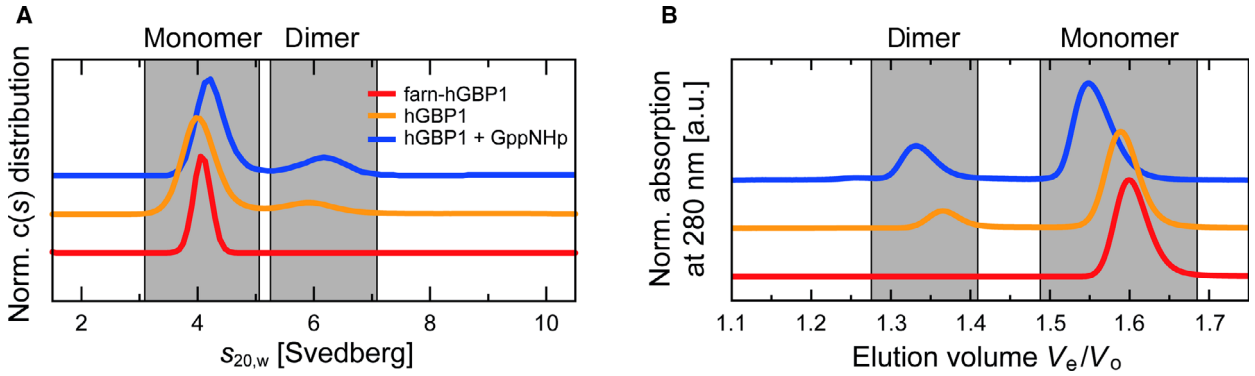

Fig. 3. Distribution profiles obtained from AUC and SEC measurements of farn-hGBP1 (red), hGBP1 (orange) and hGBP1 with 0.2 mM GppNHp (blue). (A) *c*(*S*) distribution measured by AUC. (B) Size-exclusion elution chromatogram monitored at 280 nm.

Table 2. Obtained results from SEC experiments.

	Monomer			Dimer		
	M_m [kDa]	R_h [nm]	Fraction [%]	M_m [kDa]	R_h [nm]	Fraction [%]
farn-hGPB1 13.57 mg·mL^{-1}	72.83	3.77	100	–	–	–
hGPB1 2.4 mg·mL^{-1}	85.83	3.82	85	236.40	5.01	15
hGPB1 + 1 mM GppNHp2.4 mg·mL^{-1}	103.01	4.01	76	274.72	5.22	24
SoMo1DG3/1F5N – 2BC9	69.17	3.79	–	138.34	5.3	–

the main peak of hGBP1 is also in the radius range of a monomer, but slightly larger than farn-hGBP1. In the presence of GppNHp, the R_h values of 4.01 and 5.22 nm are shifted and indicative of a structural expansion of hGBP1 upon GppNHp binding. Additionally, a small third fraction due to higher oligomers or aggregates is visible in the elution profiles (volume fraction of less than 2%) that we have neglected in our analysis and discussion.

For further analysis of the oligomeric state of hGBP1 in solution, we performed AUC experiments. Using AUC, we obtain physical parameters calculated from hydrodynamic measurements, for example, the sedimentation coefficient $s_{20,w}$, which gives additional information on conformational changes. The frictional ratio f/f_0 is informative on protein globularity and is used to calculate the molecular mass of the separated species based on f/f_0 which was assumed to be equal for all fitted species. Sedimentation velocity analysis of hGBP1 confirms the observed distribution of different oligomeric states even in the absence of nucleotides for hGBP1. The AUC experimental data are evaluated as described before, importantly they are resolved into up to three different species, which are present in solution during the AUC run. Measured AUC absorption data of nucleotide-free hGBP1 and in the presence of GppNHp are shown in Fig. 4. The results of the *c*(*s*) distribution analysis with a weight averaged f/f_0 ratio are depicted in Fig. 3A. Sedimentation coefficients, frictional ratios and molecular masses obtained from the distribution analysis are reported in Table 3 together with theoretical values of the monomer (pdb ID 1DG3) and dimer model (1F5N-2BC9) calculated with SoMo.

As in the case of SEC profiles, we observe a single distribution peak of farn-hGBP1, while two distinct peaks are found for nonmodified hGBP1 in the presence and absence of GppNHp (Fig. 3). A third minor peak is found for the nonmodified hGBP1. The two main peaks correspond to the monomeric and dimeric forms of the protein with molecular masses of 59.0–61.6 kDa for the monomer and 106.0–110.0 kDa for the dimer, see Table 3. The third minor AUC distribution peak is always around 9.2–9.6 S corresponding to a molecular weight of around 225 kDa under the assumption of the same f/f_0 value for all three species.

The obtained *c*(*s*) distribution for farn-hGBP1 always consists of only one peak (100% peak 1 as shown in Fig. 3A) corresponding to the monomeric protein for all measured conditions. The theoretical sedimentation coefficient of the monomeric crystal structure (pdb ID 1DG3) as calculated using SoMo is 3.96 S being almost identical with experimentally determined sedimentation coefficients of the

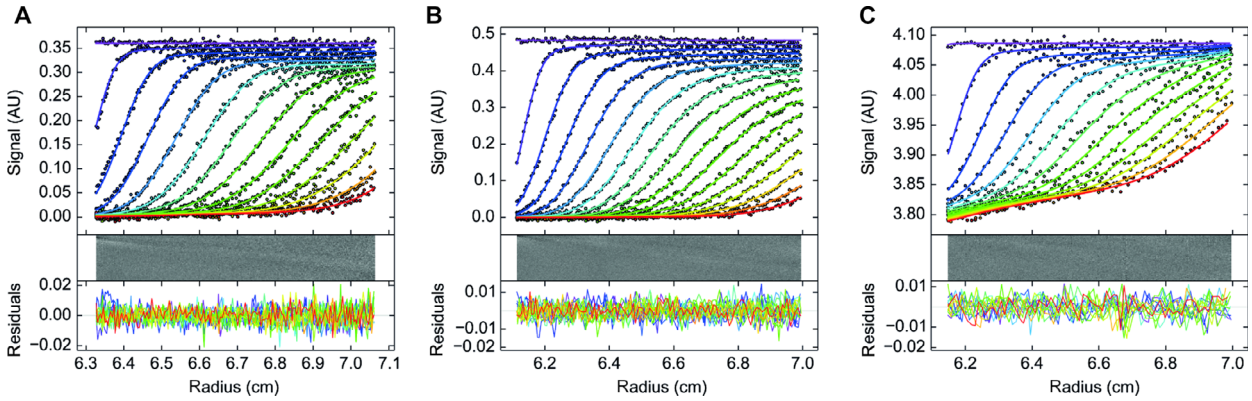

Fig. 4. Analytical ultracentrifugation absorption data from sedimentation velocity experiments. Time-resolved absorption traces are colour coded from purple (t = 0 h) to red (latest scan, $t \cong 5$ h) and corresponding fits are plotted as solid lines. (A) 4 mg·mL^{-1} farn-hGBP1. (B) 2 mg·mL^{-1} hGBP1. (C) 2 mg·mL^{-1} hGBP1 + 0.2 mM GppNHp.

Table 3. Results obtained from AUC experiments.

	Monomer			Dimer		
	M_m [kDa]	$s_{20,w}$/frict. ratio	Fraction [%]	M_m [kDa]	$s_{20,w}$/frict. ratio	Fraction [%]
2 mg·mL^{-1} farn-hGPB1	61.6	4.11 S/1.35	100	–	–	–
2 mg·mL^{-1} hGPB1	59.0	4.05 S/1.30	82	106.0	6.10 S/1.30	15
2 mg·mL^{-1} hGPB1 + 0.2 mM GppNHp	60.7	4.22 S/1.14	76	110.0	6.91 S/1.14	24
SoMo1DG3/1F5N – 2BC9	65.9	3.96 S/1.44	–	127.8	5.61 S/1.58	–

Species between 3 and 5 S are classified as monomer, between 5 and 7 S as dimer.

monomeric farn-hGBP1 and hGBP1 in the absence of nucleotide with 4.11 and 4.05 S respectively. The measured sedimentation coefficient of hGBP1 in the presence of GppNHp is 4.22 S being larger than that of the crystal structure, which indicates a modified conformation or altered hydration shell of the hGBP1 monomer due to GppNHp binding. The theoretical sedimentation coefficient of the hGBP1 dimer model 1F5N-2BC9 is 5.61 S. The experimentally determined sedimentation coefficients of the hGBP1 dimers in the absence and presence of nucleotide are larger than the theoretical value of the dimer model indicative of a different shape of the hGBP1 dimer in solution. The experimental value of the hGBP1 dimer in the presence of GppNHp appears to be larger than that in nucleotide-free solution indicative of structural rearrangements induced by GppNHp binding as well.

The frictional ratio f/f_0 reflects both the shape and hydration of the protein molecule and can be considered as an approximate measure of the protein globularity. Here, a similar frictional ratio with 1.35 of farn-hGBP1 and 1.30 of nucleotide-free hGBP1 is observed, while GppNHp results with 1.14 in a smaller f/f_0 value of hGBP1. The smaller ratio could be due to the weight averaging of f/f_0 in the $c(s)$ analysis and is, therefore, not further discussed.

Structural investigations by SAXS

Small-angle X-ray scattering experiments were performed to gain structural information of farn-hGBP1 and hGBP1 in solution at low resolution. We performed SEC-SAXS experiments, where monomers, dimers and higher order oligomers are separated on a SEC column that is directly connected to the SAXS instrument. SEC elution profiles of the monomer and dimer fractions overlaid with fitted radii of gyration R_g and forward scattering $I(0)$ from each recorded SAXS frame in the peak regions are shown in Fig. 5. Resulting SAXS data of hGBP1 and farn-hGBP1 monomers and dimers are presented in Fig. 6. Primary physical parameters were calculated from the SEC-SAXS data of the hGBP1 and farn-hGBP1 monomers and the hGBP1 dimers as described in *Material and Methods*. Radii of gyration R_g, maximal protein dimensions D_{max}, Porod volumes V_{Porod}, volumes of correlation V_c and experimental molecular masses M_m determined from V_{Porod} and V_c as well as the

theoretical molecular mass calculated from the amino acid sequence are summarized in Tables 4 and 5.

Solution structures of hGBP1 and farn-hGBP1 monomers

At first glance, the measured SEC-SAXS monomer scattering curves of farn-hGBP1 and hGBP1 are of similar shape for all conditions, see Fig. 6. The black crosses in the normalized Kratky plots of hGBP1 monomer and dimer at the position ($\sqrt{3}$, 1.104) – see middle panels in Fig. 6 indicate the position at which a globular monodomain protein that fulfils the Guinier approximation would have its maximum in a normalized Kratky plot [16]. The deviation of the peak positions of the hGBP1 monomer and dimer from that ideal value are related to the asymmetry of the protein and potentially also due to the intrinsic flexibility of hGBP1 [16]. Subtle structural differences are observed when considering the experimentally determined R_g and D_{max} values. The Guinier analysis confirms the earlier result by SEC and AUC that farn-hGBP1 has the most compact shape with a real space R_g of 3.85 nm of the monomer. The nucleotide-free hGBP1 monomer has a R_g derived from Guinier analysis of 3.89 nm, which is in a similar range as the farn-hGBP1 radius. The hGBP1 monomer in the presence of GppNHp, however, is more extended with a R_g of 4.49 nm. That observation is also visible in the determined D_{max} values. The SEC-SAXS data of the monomeric structures confirm the previous observations by SEC and AUC of similar shapes of the farn-hGBP1 and nucleotide-free hGBP1 monomer, whereas GppNHp-bound hGBP1 monomer is more extended and structurally perturbed. Another hint for structural rearrangements next to the enlarged R_g in the presence of GppNHp is the volume of correlation change (Table 4). With 547.17 Å^2 for farn-hGBP1 and 570.21 or 610.35 Å^2 for hGBP1 without nucleotide or with GppNHp, respectively, V_c deviates by 4% or 12% from the most compact conformation, which is the farn-hGBP1 monomer.

To investigate, whether the farn-hGBP1 and hGBP1 monomers are similar to the reported crystal structure (pdb ID 1DG3), we first calculated the theoretical SAXS pattern of the monomeric crystal structure using the program CRYSOL and fitted the theoretical scattering curve to the measured SEC-SAXS data of the different monomers (Fig. 7A). Concerning farn-hGBP1 in nucleotide-free solution, the fit yields a good agreement with the experimental data (χ^2 = 2.61). In comparison to farn-hGBP1, nucleotide-free hGBP1 has a larger χ^2 value of 15.06 showing that the conformation

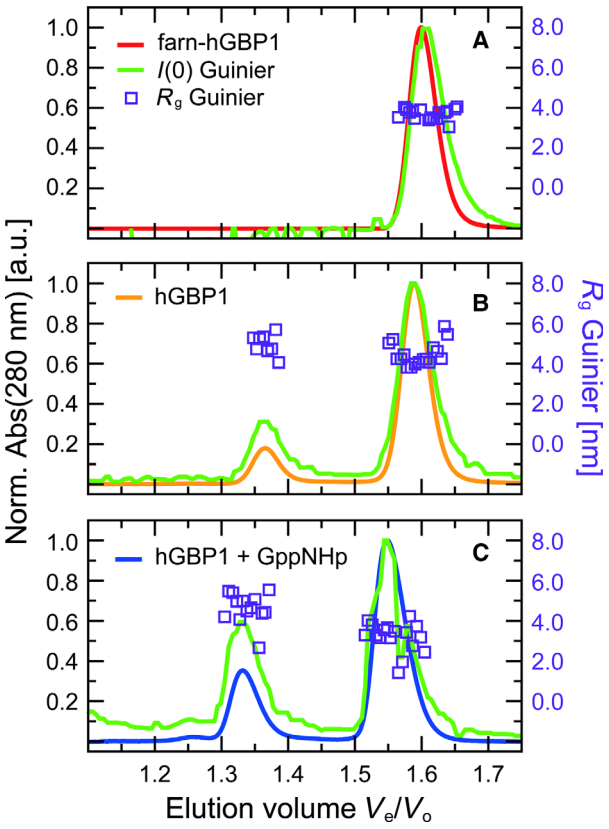

Fig. 5. Size-exclusion chromatography-SAXS plot of protein absorbance at 280 nm, $I(0)$ and R_g as function of measurement time/elution volume. $I(0)$ is normalized to absorbance maxima of the monomeric elution fraction. (A) farn-hGBP1. (B) hGBP1. (C) hGBP1 with 0.2 mM GppNHp.

in solution is different from the rigid crystal structure. Concerning hGBP1 in the presence of GppNHp, the fit quality is very poor (χ^2 = 636.12) and the residuals shown in Fig. 7A at the bottom reveal significant deviations between the theoretical curve and the measured SAXS data. Structural perturbation of GppNHp-bound monomeric hGBP1 is also visible in the larger R_G and R_h values (see Tables 1, 2 and 4). The analysis of the molecular mass of the monomers for all conditions shows a deviation from the expected theoretical value of 69.17 kDa by 5–8%, which is an expected range for small-angle scattering data analysis [17] and underlines the correct classification of this species as monomer.

EOM modelling was performed as a next step. Good fits to the SEC-SAXS in the q-range up to 0.2 Å^{-1} were obtained (χ^2 = 1.10 for farn-hGBP1, χ^2 = 1.69 for hGBP1, and χ^2 = 46.35 for hGBP1+GppNHp). Experimental SEC-SAXS data with EOM fits are shown in Fig. 8A. From EOM conformational ensemble

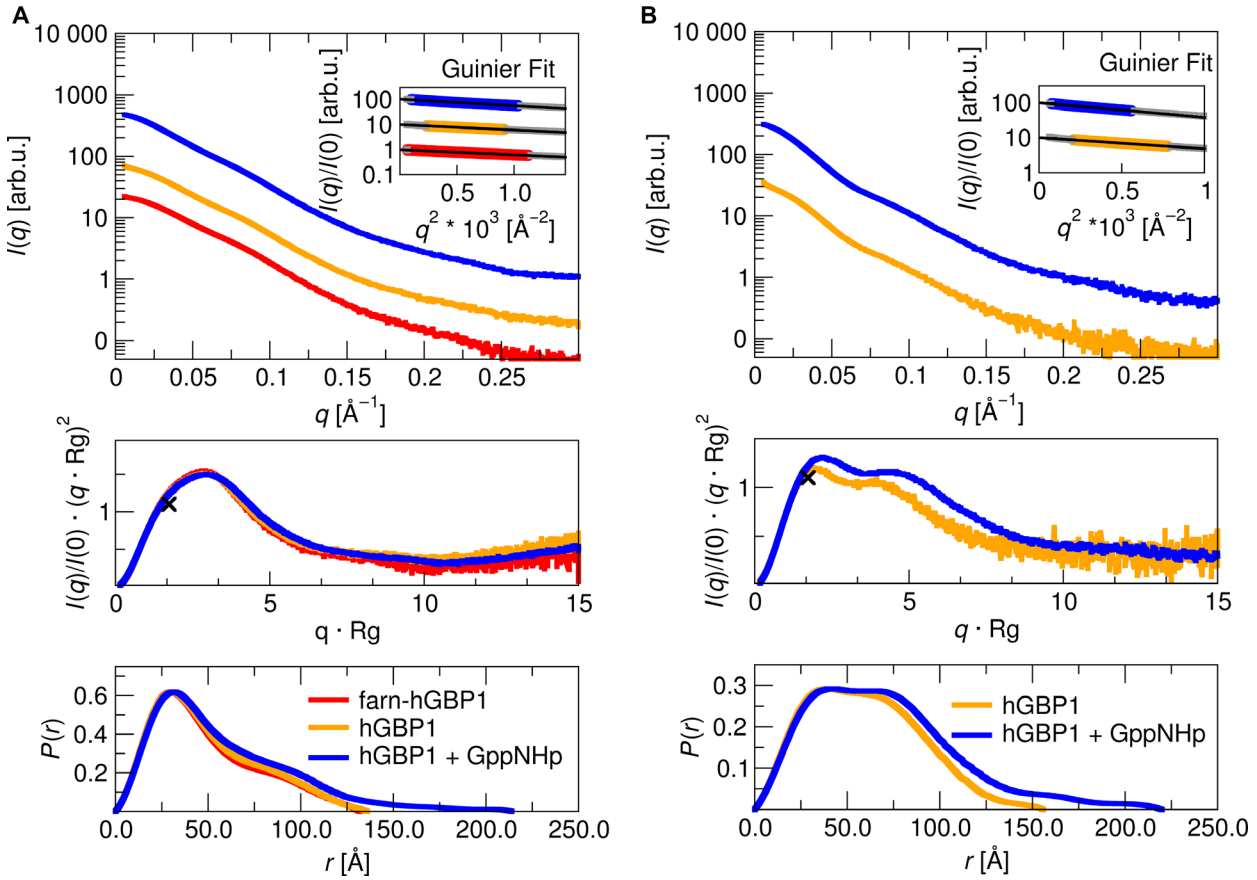

Fig. 6. Experimental scattering results from SEC-SAXS experiments with hGBP1. Farn-hGBP1 shown in red, hGBP1 in orange and hGBP1 + 0.2 mM GppNHp in blue. First panels contain Log-Lin representation of binned raw data with inset showing the Guinier fit for determination of R_g. Second panels show the normalized Kratky representation of the raw data and the third panels the real space distribution function $P(r)$. The black crosses in the normalized Kratky plots of hGBP1 monomer and dimer at the position ($\sqrt{3}$, 1.104) indicate the peak position that would be expected for a globular monodomain protein that fulfils the Guinier approximation. Data of Log-Lin plots and in Guinier representation are y-shifted for clarity. (A) Binned scattering raw data eluting from SEC in the range of 1.5–1.7 V_e/V_o are classified as monomers. (B) Binned scattering raw data eluting from SEC in the range of 1.3–1.4 V_e/V_o are classified as dimers.

analysis, distributions of radii of gyration R_G and maximal structural dimensions D_{max} are derived and are shown in Fig. 9. For farn-hGBP1 and hGBP1, the best structural models are found in two clusters with R_G around 35 and 45 Å, whereas in the presence of GppNHp the clusters are shifted to higher R_G values. In the D_{max} distribution, the values of farn-hGBP1 and hGBP1 are single peaked, while the D_{max} distribution hGBP1+GppNHp is significantly broadened demonstrating a larger conformational flexibility of hGBP1+GppNHp as compared to farn-hGBP1 and nucleotide-free hGBP1. EOM additionally provides a parameter R_{flex} to allow a quantitative characterization of the distributions. R_{flex} is coupled with the entropy of the protein and, therefore, to the flexibility of the system. A low entropy content corresponds to a low R_{flex} value. Highly flexible proteins on the other hand have high R_{flex} values. A theoretical protein having Gaussian-like chain statistics would have R_{flex} = 100% [18]. Moreover, R_{flex} parameters calculated by (Ensemble Optimization Method) EOM allow to quantify the flexibility of the proteins in comparison to the generated structural pool. The obtained R_{flex} parameters are 76.2% for farn-hGBP1, 80.6% for nucleotide-free hGBP1 and 81.5% for hGBP1+GppNHp, while the corresponding value of the structural pool is 91.3%. As stated before, R_{flex} of 100% would correspond to a Gaussian-like distribution of structural parameters with randomly aligned regions in solution. Those R_{flex} values are indicative of a less flexible farn-hGBP1 and significantly more flexible hGBP1 monomers without the farnesyl group being attached [18].

Table 4. Primary physical parameters derived from SAXS data of farn-hGBP1 and hGBP1 monomers.

Monomer			
Software	farn-hGBP1	hGBP1	hGBP1 + GppNHp
PRIMUS/ATSAS			
R_g from Guinier analysis [nm]	3.85 ± 0.05	3.89 ± 0.06	4.49 ± 0.04
R_g from $P(r)$ [nm]	3.97	4.02	4.79
D_{max} from $P(r)$ [nm]	13.11	13.44	19.99
Porod volume [nm^3]	102.1	105.7	119.6
M_m from Porod [kDa]	63.82	66.08	74.78
Deviation exp. M_m from theor. MW	8%	5%	8%
SCÅTTER			
M_m from Q_R [kDa]	64.00	65.30	74.00
Deviation exp. from theor. M_m	8%	6%	7%
R_g from Guinier analysis [nm]	3.80	3.88	4.09
Volume of correlation V_c [Å^2]	547.17	570.21	610.35
PROTPARAM			
M_m theor. [kDa]	69.17	69.17	69.17

Table 5. Primary physical parameters derived from SAXS data of the hGBP1 dimers.

Dimer		
Software	hGBP1	hGBP1 + GppNHp
PRIMUS/ATSAS		
R_g from Guinier analysis [nm]	4.79 ± 1.56	5.45 ± 0.16
R_g from $P(r)$ [nm]	4.72	5.73
D_{max} from $P(r)$ [nm]	15.61	22.00
Porod volume [nm^3]	211.2	269.6
M_m from Porod [kDa]	132.01	168.49
Deviation exp. from theor. M_m	5%	18%
SCÅTTER		
M_m from Q_R [kDa]	130.95	159.38
Deviation exp. from theor. M_m	6%	13%
R_g from Guinier analysis [nm]	4.68	5.44
Volume of correlation V_c [Å^2]	868.57	1033.11
PROTPARAM		
M_m theor. [kDa]	138.34	138.34

Structural rigid-body modelling using SASREF was performed as well and gave excellent fits up to $q = 0.3$ Å^{-1} based on the residual deviation of the fit from the experimental data ($\chi^2 = 3.02$ for farn-hGBP1, $\chi^2 = 1.39$ for hGBP1, but $\chi^2 = 41.48$ for hGBP1+GppNHp). Experimental SEC-SAXS data of the monomers and SASREF fits are shown in Fig. 10. Using SASREF, only a single structure is refined against the SEC-SAXS data, while for EOM analysis a conformational ensemble is generated. However, SASREF models allow to visualize the measured SEC-SAXS data as average structural models. Rigid-body modelling fails for larger q-ranges due to local structural perturbations that cannot be modelled using only rigid-body domains. Obtained structural SASREF models are shown in Fig. 10 as well. While for farn-hGBP1, a structure is obtained that is very similar to the crystal structure, the obtained models for nucleotide-free hGBP1 and hGBP1+GppNHp show the structural perturbation of the protein directly. The conformational flexibility of hGBP1 monomer is due to a reorientation of helices 12 and 13 that is more pronounced in the presence of GppNHp.

Solution structures of dimeric hGBP1

The second SEC-SAXS elution peak, which was further analysed, is in the range of 1.32–1.40 V_e/V_o eluting from the SEC column and only appears for nonfarnesylated hGBP1 in nucleotide-free buffer or in the presence of GppNHp. The analysis of the molecular mass by Porod volume and the volume of correlation confirms that this is a dimeric species of hGBP1 with a deviation from the expected theoretical dimer weight of 138.34 kDa by 5–18% (Table 5). Another hint for the dimeric nature of this species is the comparison of absorption to forward scattering intensity (Fig. 5) where $I(0)$ is always higher by approximately a factor of 2 in this region compared to absorption at 280 nm when both are normalized to 1 at the maximum peak position. The absorption is indicative for the total number of proteins in solution, hence a bulk property. The forward scattering $I(0)$, however, is proportional to the number of electrons contained in a scattering volume. This means that the molecular mass is higher in this eluting species by approximately a factor of 2 compared to the first monomer peak, to which the chromatogram is normalized. Considering the hGBP1 dimers, we find similar radii of gyration and maximal dimensions indicative of similar dimer structures in the presence and absence of nucleotide.

As a first step, we calculated the theoretical scattering function of the dimer model (see Fig. 1B) using the program CRYSOL and compared the theoretical fits to the measured SEC-SAXS data of the hGBP1 dimers, shown in Fig. 7B. From a visual inspection of the fits, it is already clear that the dimer model does not reproduce the measured SEC-SAXS data. This is particularly clear for the double peak structure visible in the Kratky plot (middle panel of Fig. 7B) that is not reproduced at all by the theoretical model. That observation is corroborated by the obtained χ^2 values

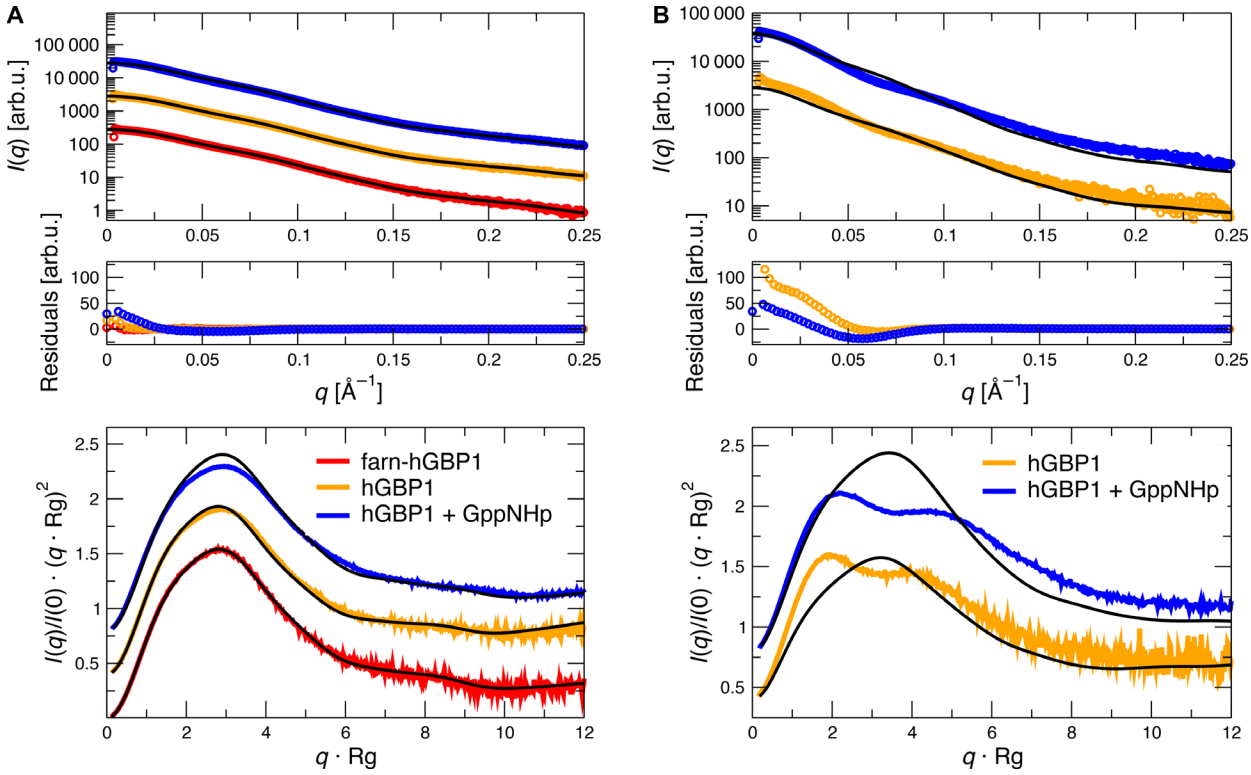

Fig. 7. CRYSOL fit results. Experimental SEC-SAXS data are represented as dots (farn-hGBP1 in red, hGBP1 in orange and hGBP1 with GppNHp in blue) and CRYSOL fits drawn as solid lines. First panels show Log-Lin representations of the scattering raw data, second panels show the fit residuals and the third panels show the normalized Kratky representation. (A) Monomer scattering and fit. Crystal structures of full-length hGBP1 (pdb ID 1DG3) and in the presence of GppNHp (pdb ID 1F5N) were used for fitting. The resulting fit χ^2 values are 2.61 for farn-hGBP1, 15.06 for hGBP1 and 636.12 for hGBP1 in the presence of GppNHp. (B) Dimer scattering and fit. Aligned dimeric structure 1F5N-2BC9 as shown in Figure 1 B was used for fitting. Fit χ^2 results are 12.84 for hGBP1 and 1057.23 for hGBP1 in the presence of GppNHp.

of 12.84 and 1057.23 for hGBP1 dimer in nucleotide-free and GppNHp solution, respectively, and by the residuals that show large deviations between theoretical model and experimental data.

EOM analysis was performed as a next step and the experimental SEC-SAXS data with EOM-based fits are shown in Fig. 8B in the q-range up to 0.2 Å^{-1}. Obtained *R*flex-values are 0.85 and 1.49 for hGBP1 and hGBP1+GppNHp dimers, respectively, indicative of good fits to the data. Obtained R_g and D_{max} distributions are presented in Fig. 9B and D. Two differently occupied clusters of dimer conformations are obtained indicative of two distinct structural states. For hGBP1+GppNHp, the major peak is significantly broadened, indicative of enhanced structural flexibility as compared to the nucleotide-free hGBP1 dimer. The obtained R_{flex}-values corroborate the larger structural plasticity of the hGBP1+GppNHp dimer with R_{flex} = 74.1% and 80.6% for nucleotide-free and GppNHp solution, respectively, while R_{flex} = 90.4% corresponds to the flexibility of the generated structural pool.

Using the rigid-body modelling approach from SASREF, dimeric hGBP1 constructs are calculated and presented in Fig. 11 together with the experimental SEC-SAXS data in the q-range up to 0.3 Å^{-1}. During SASREF modelling the structural constraint was considered that the helices 13 remain in contact with each other, which is based on the previous FRET and EPR study by Vöpel *et al.* [11]. The χ^2-values of the fits are 0.91 and 6.40 for hGBP1 and hGBP1+GppNHp dimers, respectively, indicative of good fits to the data as well. The theoretical curves represent the characteristic double peak of the Kratky plots very well. Obtained structural models of both hGBP1 dimers are shown in Fig. 11B. Both models show a perturbed and flexible dimer structure with opened middle domains.

Validation of structural rigid-body models by their hydrodynamic properties

To validate the obtained rigid-body models that have been obtained by SAXS, we calculated their

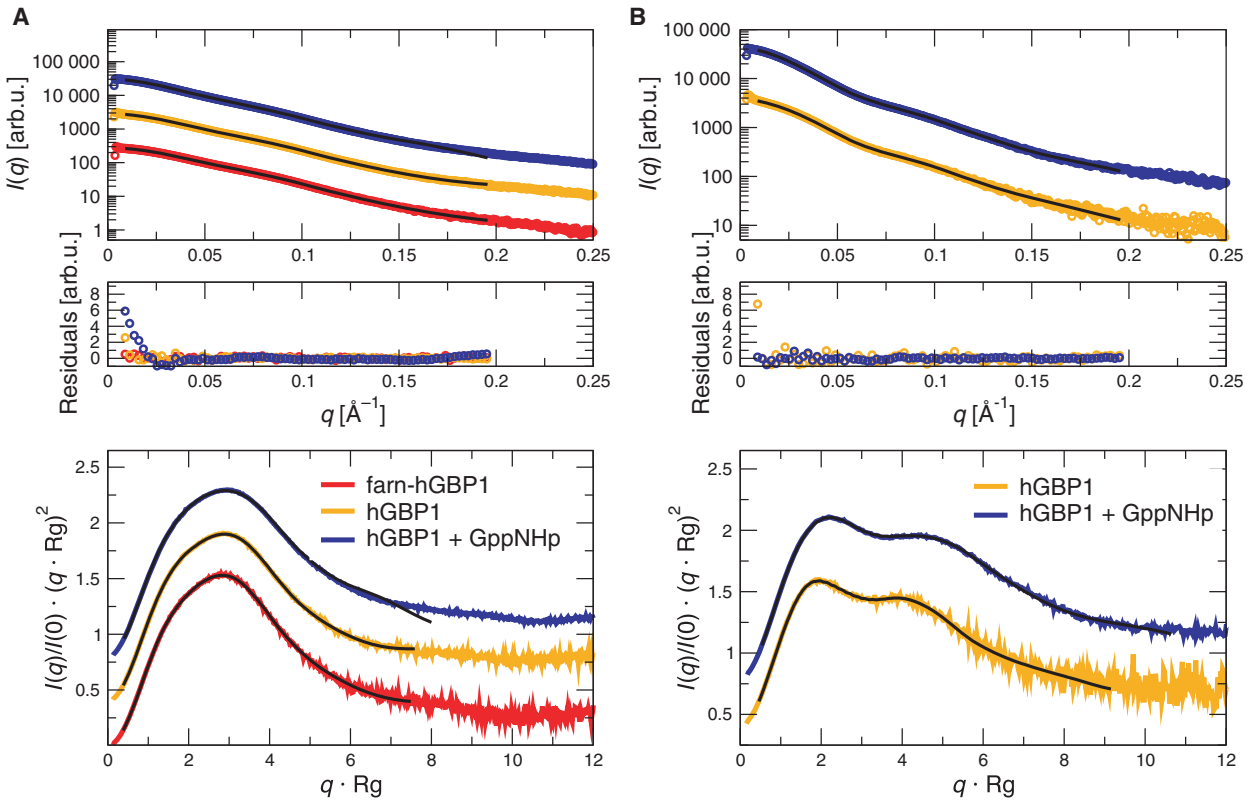

Fig. 8. EOM fit results of scattering data from SEC-SAXS experiments. Experimental SEC-SAXS data are represented as dots (farn-hGBP1 in red, hGBP1 in orange and hGBP1 with GppNHp in blue) and obtained theoretical scattering from EOM fits drawn as solid lines. First panels show Log-Lin representations of the scattering raw data, second panels show the fit residuals and the third panels show the normalized Kratky representation. (A) Monomer scattering and fit results with χ^2 values 1.10 for farn-hGBP1, 1.69 for hGBP1 and 46.35 for hGBP1 in the presence of GppNHp. (B) Dimer scattering and fit results with χ^2 values 0.85 for hGBP1 and 1.49 for hGBP1 in the presence of GppNHp.

hydrodynamic parameters using the program SOMO and compared the obtained theoretical values with the corresponding experimental parameters. Calculated sedimentation coefficients, hydrodynamic radii as well as theoretical radii of gyration of all obtained monomer and dimer structures are summarized and compared to the experimentally determined parameters obtained by AUC, SEC and SEC-SAXS in Tables 6 and 7. Good and reasonable agreement between calculated R_h and R_g values and corresponding experimental parameters is found for all monomer and dimer models. Calculated sedimentation coefficients of hGBP1 and farn-hGBP1 monomers are systematically underestimated. For hGBP1, the calculated dimer structure shows similar hydrodynamic properties compared to the earlier SEC and AUC experiments. In the presence of GppNHp, the parameters of the calculated dimer systematically deviate from the experimentally determined sedimentation coefficient.

Discussion

Previous studies have reported that hGBP1 is a flexible molecule that can undergo large conformational changes upon activation by nucleotides. This was proven, for example, with biochemical assays like amino acid accessibility on the surface by Vöpel *et al.* [19]. In that study by Vöpel *et al.*, it has been shown that in the presence of GppNHp, the buried cysteines are better accessible compared to the control condition in the presence of GMP or nucleotide-free solution, which is indicative of higher flexibility in the protein in the presence of GppNHp. Moreover, in the presence of GTP, the authors proposed that a cysteine becomes accessible, which is located on helix 4′ (see Fig. 1) and is usually buried between LG domain and C-terminal helices 12/13. This movement of helix 4′ was also indicated from the crystallographic dimer structures of the LG domains as helix 4′ would clash with helix 12/13 when the full-

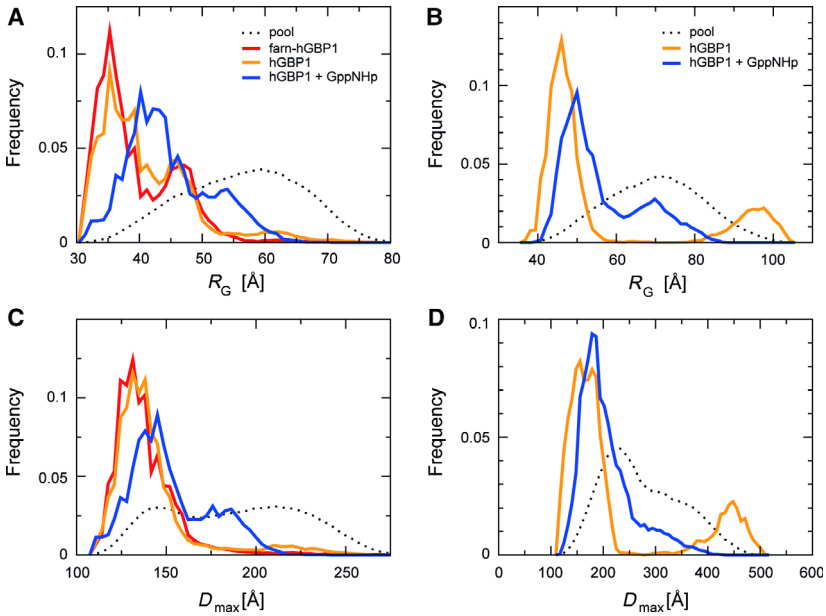

Fig. 9. Distribution of R_g and D_{max} obtained from EOM modelling. Farn-hGBP1 (red), hGBP1 (orange) and hGBP1 + GppNHp (blue). (A) Distribution of frequencies of radii of gyration R_g of monomers for the different conditions. (B) Distribution of frequencies of radii of gyration R_g of dimers for the different conditions. (C) Distribution of frequencies of maximal dimensions D_{max} of monomers for the different conditions. (D) Distribution of frequencies of maximal dimensions D_{max} of dimers for the different conditions.

length crystallographic structure is aligned to it. Therefore, it has been proposed that the LG domain and helices 12/13 move away from each other in the course of GTP hydrolysis. In later studies using FRET and EPR, it was shown that helix 13 detaches from helix 12, which allows helix 13 to establish a second dimer interface of two hGBP1 proteins [11]. Recent studies on farn-hGBP1 – as found under physiological conditions – illustrate that farn-hGBP1 can build up large polymeric structures that are relevant for membrane interactions [12]. For the mechanism of polymerization of farn-hGBP1, it was suspected that a large rearrangement by opening and particularly releasing the α12/13 domain upon GTP binding is necessary [11,13,19] and a nucleotide-dependent release of the farnesyl anchor mediates the opening of hGBP1 and allows hydrophobic interactions [12].

Our study on hydrodynamic and structural differences between farn-hGBP and hGBP shows that farn-hGBP1 under nucleotide-free conditions is present as monomer only, while hGBP1 both under nucleotide-free and GppNHp solution conditions is present as a monomer–dimer equilibrium. The solution structure of farn-hGBP1 monomer is in a compact crystal-like conformation as seen by its hydrodynamic behaviour and its solution structure. Without the farnesyl moiety, the hGBP1 monomer shows structural perturbations as compared to the crystal structure with increased conformational flexibility, which is strongly enhanced upon GppNHp binding. Rigid-body models of non-modified hGBP1 derived from SAXS data suggest that observed structural plasticity is caused by α-helices 12 and 13 that detach from the rest of the protein being significantly more flexible for the GppNHp-bound hGBP1 monomer. The solution structures of hGBP1 and farn-hGBP1 determined by SAXS are cross-validated with their experimentally determined hydrodynamic properties as measured by DLS and AUC, see Tables 7 and 8.

A further novel result that we report in our study is the fact that a dimeric hGBP1 structure is found for nonmodified hGBP1 in the absence and presence of GppNHp. Up to now, it has been assumed that non-modified nucleotide-free hGBP1 is entirely monomeric in solution, while hGBP1 in the presence of GppNHp forms purely dimers. Our experimental results demonstrate that this is not the case, the monomer–dimer equilibrium of hGBP1 is established independently of the presence of nucleotides. Solution structures of dimeric hGBP1 are not in agreement with the dimer model that is based on available crystal structures (see Fig. 1B). Instead, the hGBP1 dimer in solution shows structural perturbations similar to its monomeric state: α-helices 12/13 are detached from the protein and rigid-body modelling agrees with a dimerization interface formed by two α13 helices of two hGBP1. The double peak of dimeric hGBP1 visible in the Kratky peak is the characteristic feature of the protein in solution. It can only be reconstructed by structurally perturbed and opened hGBP1 dimer models. Furthermore, structural flexibility of hGBP1 dimer in the presence of GppNHp is increased as compared to the nucleotide-free state, which is also observed for the hGBP1 monomer.

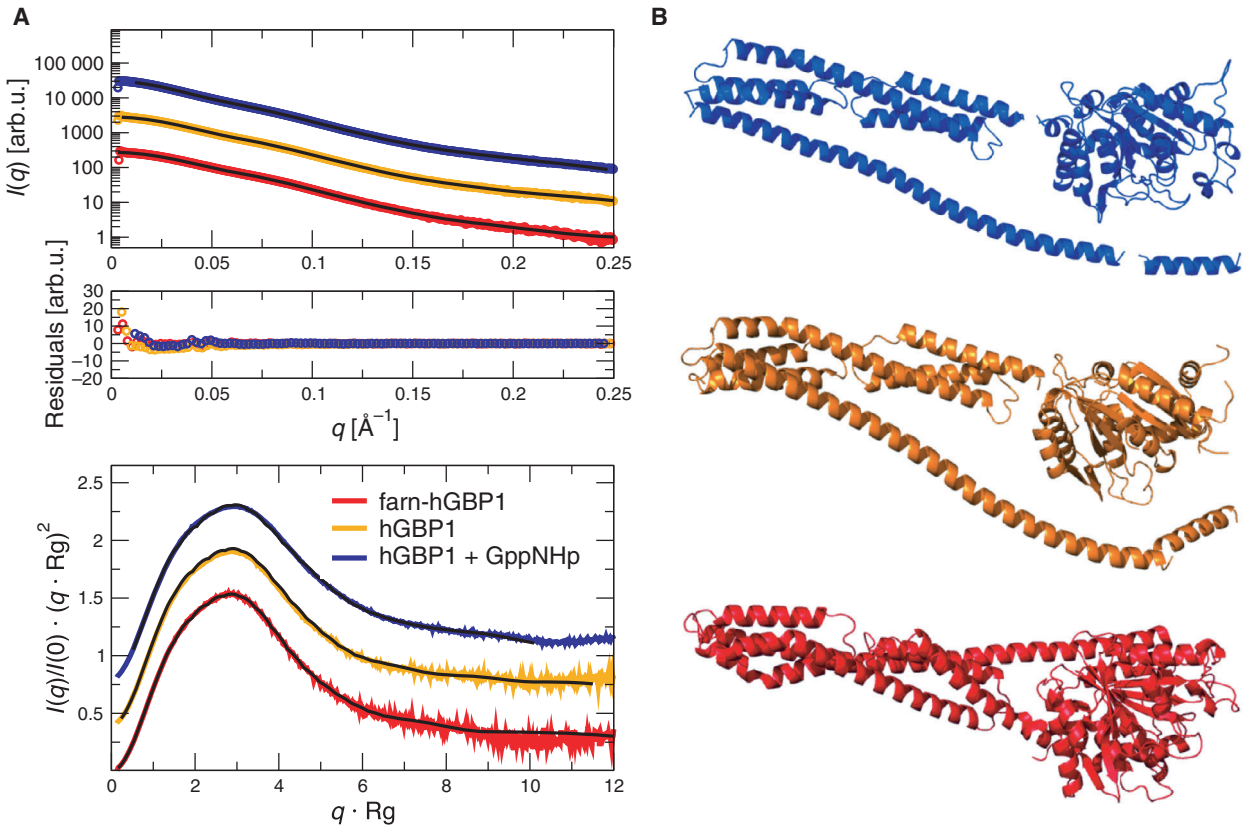

Fig. 10. SASREF fit results of monomer scattering data from SEC-SAXS experiments. (A) Experimental SEC-SAXS data are represented as dots (farn-hGBP1 in red, hGBP1 in orange and hGBP1 with GppNHp in blue) and obtained theoretical scattering from SASREF fits drawn as solid lines. First panel shows Log-Lin representations of the scattering raw data, second panel shows the fit residuals and the third panel shows the normalized Kratky representation. Monomer scattering and fit results with χ^2 values 3.02 for farn-hGBP1, 1.39 for hGBP1 and 41.48 for hGBP1 in the presence of GppNHp. (B) Monomer structural models obtained from rigid-body modelling (farn-hGBP1 in red, hGBP1 in orange and hGBP1 with GppNHp in blue).

As the appearance of dimers is completely vanished in the presence of farnesylation, this post-translational modification seems to be important as a safety mechanism to prevent uninduced signal transduction under biological conditions in cells. The earlier described dimers formed via the LG interface can already occur under nucleotide-free conditions of nonmodified hGBP1. This observation underlines and confirms the earlier proposed dimerization mechanism of the previously described domain movements of α12/13 domain upon GTP binding. The dimeric fractions of hGBP1 are surprisingly already present under nucleotide-free conditions in the chosen concentration range that is appropriate for SEC, AUC and SAXS measurements. The high flexibility of the dimer as shown from EOM analysis could be very important to mediate further oligomerization and demonstrate the first molecular steps that occur during the supramolecular assembly process of farn-hGBP1 in the presence of GTP and GDP AlFx as already observed before. This principle of conformational flexibility for signal transduction has been observed for light-sensitive signalling proteins as well [20,21]. Opened hGBP1 dimer structures would enable the formation of circular nucleation discs of farn-hGBP1 with fully extended hGBP1 and LG domains pointing at the outside of the oligomer, while the farnesyl group is located in the centre of the disc as previously suggested based on cryo-TEM images [12]. Future work will be directed to investigate the occurrence of structural perturbations induced by nucleotides during the assembly process of farn-hGBP1 to the observed supramolecular structures.

Materials and methods

Expression and purification of unmodified and farnesylated hGBP1

Unmodified and farnesylated hGBP1 were purified as described earlier [8,22]. In short, for expression of farnesylated

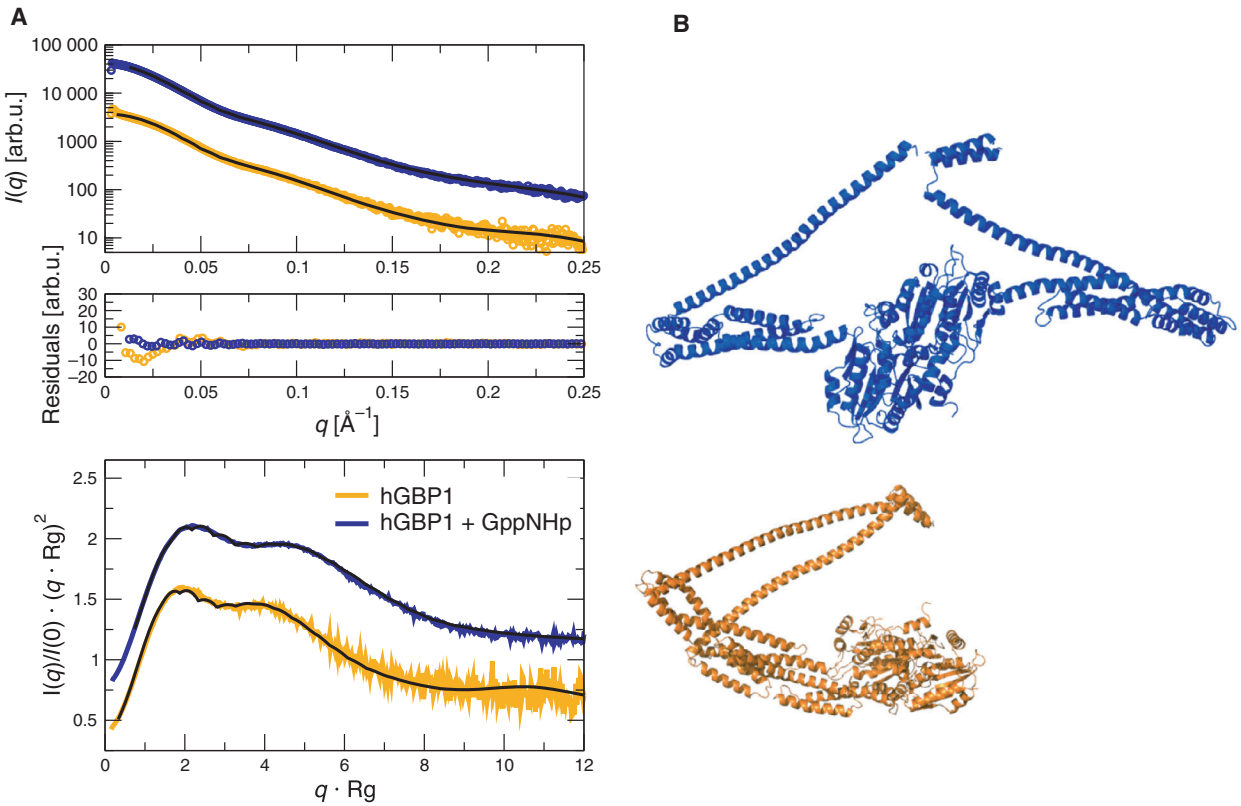

Fig. 11. SASREF fit results of dimer scattering data from SEC-SAXS experiments. (A) Experimental SEC-SAXS data are represented as dots (hGBP1 in orange and hGBP1 with GppNHp in blue) and obtained theoretical scattering from SASREF fits drawn as solid lines. First panel shows Log-Lin representations of the scattering raw data, second panel shows the fit residuals and the third panel shows the normalized Kratky representation. Dimer scattering and fit results with χ^2 values 0.91 for hGBP1 and 6.40 for hGBP1 in the presence of GppNHp. (B) Dimer structural models obtained from rigid-body modelling (hGBP1 in orange and hGBP1 with GppNHp in blue).

Table 6. Hydrodynamic and structural parameters of best models of farn-hGBP1 and hGBP1 monomers compared to measured parameters by AUC, SEC and SEC-SAXS.

	s (20,w) Experimental/ Model result	R_g [nm] Experimental/ Model result	R_h [nm] Experimental/ Model result
farn-hGBP1	4.11 S/3.96 S	3.85 nm/4.00 nm	3.77 nm/3.79 nm
hGBP1	4.05 S/3.61 S	3.89 nm/4.00 nm	3.82 nm/3.96 nm
hGBP1 + GppNHp	4.22 S/3.64 S	4.49 nm/4.35 nm	4.01 nm/4.16 nm

Crystal structure (pdb ID PDB 1DG3) used for farn-hGBP1, SASREF rigid-body models used for monomeric nonmodified hGBP1 species.

Table 7. Hydrodynamic and structural parameters of best models of hGBP1 dimers compared to measured parameters by AUC, SEC and SAXS

	s(20,w) Experimental/ Model result	R_g [nm] Experimental/ Model result	R_h [nm] Experimental/ Model result
hGBP1	6.10 S/5.58 S	4.68 nm/4.79 nm	5.12 nm/5.11 nm
hGBP1 + GppNHp	6.91 S/5.07 S	5.45 nm/5.57 nm	5.22 nm/5.64 nm

SASREF rigid-body models used for dimeric nonmodified hGBP1.

hGBP1 (farn-hGBP1), the plasmid containing the hGBP1 gene was coexpressed with a plasmid coding for human farnesyltransferase subunits α/β. The plasmids were obtained from G. Praefcke as a friendly gift and are the same as used in earlier publications and as the full-length protein used for crystallization [6,23]. Plasmids containing hGBP1 (pQE80L) and/or farnesyltransferase subunits (pRSF-DUET1) were transformed in *Escherichia coli* BL21(DE3)-RIL cells using the heat shock method, cultivated in Terrific Broth (TB) medium supplemented with 100 μg·mL^{-1} ampicillin and/or 50 μg·mL^{-1} kanamycin, respectively, and expression was induced by the addition of 100 μM isopropyl-D-thiogalactopyranoside. After 16 h at 22 °C, cells were harvested by centrifugation at 5000 ***g*** for 20 min at 4 °C.

Table 8. Measured viscosity and density of the buffers used for AUC.

Buffer	Buffer C			Buffer C + 200 μM GppNHp		Water
Temp [°C]	10	20	22	10	22	20
Viscosity [cP]	1.380	1.050	1.002	1.546	0.987	1.002
Density [g·cm^{-3}]	1.0096	1.0079	1.0074	1.0097	1.0075	0.9982

Purification of hGBP1

Cells were resuspended in buffer containing 50 mM Tris-HCl (pH 7.9), 5 mM $MgCl_2$, 500 mM NaCl and 10% glycerol (v/v) and disrupted using a tip sonicator (Bandelin-Sonoplus, Berlin, Germany) or a French pressure cell (Thermo Scientific, Waltham, MA, USA) with a maximum pressure of 1.7 kbar at 4 °C. After centrifugation at 15 000 ***g*** for 60 min at 4 °C, the supernatant was subjected to His_6-tag affinity chromatography (HisPur Cobalt Resin, Thermo Scientific, or TALON superflow, GE Healthcare, Chicago, IL, USA). hGBP1 containing fractions were combined and ammonium sulphate was added to a final concentration of 3 M. After 10 min of stirring at room temperature, the precipitate was separated by centrifugation at 7140 ***g*** for 15 min at 4 °C. The pellet was either stored at −80 °C or directly resuspended in buffer C [50 mM Tris-HCl (pH 7.9), 5 mM $MgCl_2$, 150 mM NaCl] and applied onto a Superdex 200 26/60 column. All fractions containing monomeric hGBP1 were combined, concentrated to a final concentration of about 100 mg·mL^{-1} and frozen in liquid nitrogen for storage at −80 °C. The protein purity was analysed by SDS/PAGE (4-20% gradient gel, Expedeon).

Purification of farn-hGBP1

The purification strategy was the same as described for hGBP1, with an additional hydrophobic interaction chromatography (HIC, HiTrap Butyl HP, GE Healthcare) step for separation of unmodified from farnesylated hGBP1 after His_6-tag affinity chromatography. The HIC column was equilibrated with buffer containing high salt concentration (50 mM Tris-HCl (pH 7.9), 5 mM $MgCl_2$ and 1.2 M $(NH_4)_2SO_4$) and eluted with low salt buffer (50 mM Tris-HCl (pH 7.9), 5 mM $MgCl_2$). After His_6-tag affinity as well as after HIC chromatography, the protein containing fractions were precipitated using 3 M $(NH_4)_2SO_4$ as described for the unmodified hGBP1 before.

Sample preparation for AUC, DLS and SAXS measurements

All buffers were degassed before usage and samples were freshly prepared directly before the respective measurements. Protein concentration was determined on a NanoDrop 2000c Spectrophotometer (Thermo Scientific) using an extinction coefficient of 46 340 M^{-1}·cm^{-1} (calculated with full-length amino acid sequence of hGBP1 with His_6-tag using ProtParam on the ExPASy server).

The concentrated protein stock solution was diluted in buffer C to desired concentrations. Possible higher aggregates were removed by centrifugation at 13 400 ***g*** for 22 min at room temperature and the supernatant was used for measurements. For measurements in the presence of GppNHp, the nucleotide was added directly before the measurement at the desired concentration as indicated in the results part (either 0.2, 1.0 or 1.5 mM final nucleotide concentration) and samples were incubated 10–30 min at room temperature.

Dynamic light scattering

Translational diffusion coefficients (D_{trans}) of the different samples were measured using dynamic light scattering experiments on a Malvern Zetasizer Nano ZS instrument (4 mW He-Ne laser, λ = 633 nm, θ = 173°). At least three different protein concentrations between 0.2 and 5 mg·mL^{-1} were measured with at least 15 runs per measurement to extrapolate the translational diffusion coefficient to zero concentration $D_{trans}(conc \rightarrow 0)$. D_{trans} and Stokes radii were calculated using the standard protein analysis mode of the instrument's software which is a non-negative least squares (NNLS) analysis followed by L-curve regularizer calculation.

Analytical size-exclusion chromatography

Samples of hGBP1 were prepared as described before to final protein concentrations of 2 or 13 mg·mL^{-1} in buffer C. The samples were incubated for 30 min at room temperature before injection on the gel filtration column (Superdex 200 10/300 GL, GE Healthcare). The elution profile was monitored by absorption at 280 nm using an Äkta Purification system (FPLC, GE Healthcare). The calibration of the system was done using commercially available standard proteins (blue dextran, ferritin, catalase, conalbumin, ovalbumin) as well as BSA (monomers/dimers with 66/132 kDa) and farn-hGBP1 (monomer with 69 kDa) under the same running and buffer conditions. The calibration runs were used to determine the column-specific calibration curve. As the crystal structure of hGBP1 exists in an elongated shape, the assumption of globular eluting particles does not hold and, therefore, the molecular weight calibration is error prone (Eq. 2). We preferred to calculate

the hydrodynamic properties of the proteins as described in 4.7 *Hydrodynamic calculations* and calculate the elution profile depending on the hydrodynamic size (Stokes radius or hydrodynamic radius R_h). The obtained calibration curves can be used to calculate the molecular weight MW [kDa] (eq. 2) or R_h [Å] (Eq. 3) of the eluting species at different elution times with V_e as elution volume [mL] and V_o = 8.2 mL as void volume (R^2 = 0.96).

$$\log \mathrm{MW} = -4.53 \cdot \frac{V_e}{V_o} + 11.65 \quad (1)$$

$$\log R_h = -1.22 \cdot \frac{V_e}{V_o} + 5.58 \quad (2)$$

The oligomeric distribution was estimated by peak area integration of each peak divided by the total peak area of all peaks.

Analytical ultracentrifugation

All samples were freshly prepared for centrifugation experiments as described earlier. Sedimentation experiments were performed using a Beckman Coulter ultracentrifuge equipped with an absorption optical scanner (Optima XL-A) at 10 °C with 116,272 ***g***. The detection wavelength was chosen between 290 and 300 nm in order to keep the signal contribution from the added nucleotide small. An 8-hole titanium rotor loaded with titanium double sector cells (1.2 cm optical path length) with quartz windows had been used for the measurements. Data recording was performed after thorough thermal equilibration in intensity mode with a radial step size of 0.002 cm.

Partial specific volume $\bar{v}$ of the protein was estimated using Sednterp [24] for the protein sequence of hGBP1 with attached His-tag (0.73627 $cm^3 \cdot g^{-1}$ at 22 °C, 0.73754 $cm^3 \cdot g^{-1}$ at 20 °C and 0.73117 $cm^3 \cdot g^{-1}$ at 10 °C). Buffer viscosity and density were measured for all buffers with or without added nucleotide (Anton Paar DMA5000, Anton Paar Microviscosimeter Lovis 2000 M), see Table 8. The AUC data were analysed using the software SEDFIT with continuous $c(s)$ distribution model. The minimal chosen resolution was 0.1 S with at least s_{min} = 1 S and s_{max} = 15 S and applying a logarithmic s-space for all samples. The conventional $c(s)$ distribution as described by Schuck [25] is confined to a single frictional ratio, which is determined as a weight-average frictional ratio f/f_0 of all sedimenting material from nonlinear optimization of this parameter [26]. To simplify the comparison of the results, the obtained sedimentation coefficients are transformed to standard solvent conditions of water at 20 °C [27].

$$s_{20,w} = s_{\exp}\left(\frac{\eta_{\exp}}{\eta_{20,w}}\right)\left(\frac{1-\bar{v}_{20,w}\cdot\rho_{20,w}}{1-\bar{v}_{\exp}\cdot\rho_{\exp}}\right) \quad (3)$$

Oligomer distribution was determined from the obtained $c(s_{20,w})$ distributions. Peak maxima are determined with a threshold of 1% of the distributions maximum peak height. The peak limits are chosen by reaching a local minimum or 20% of the peak's height. The peak area is then calculated with Simpson's rule integration. For estimation of the oligomeric fraction ν, integrated peak areas of each peak are divided by the total sum of all peaks.

Small-angle X-ray scattering

Size-exclusion chromatography coupled with small-angle X-ray scattering measurements were performed at beamline BM29 at the European Synchrotron Radiation Facility (ESRF) [28] with λ = 0.992 Å as the X-ray wavelength (corresponding to an energy of 12.5 keV) in-line with a size-exclusion column (SEC) (Superdex 200 10/300 GL, GE Healthcare) [29]. The X-ray beam size at the sample position is around 700 × 700 μm^2 and a Pilatus 1M detector was used. Photon flux at sample position of BM29 is reported to be up to 10^{12} photons/s at maximal ESRF ring current [28]. Ring current of the ESRF during the SAXS experiment was 200 mA, which is the maximal current of the machine. The scattering vector q is defined as $q = 4\pi/\lambda \cdot \sin(\theta/2)$ with the incident wavelength λ and scattering angle θ. The measurements cover an effective q-range from 0.006 to 0.49 $Å^{-1}$.

All samples were prepared as described before with applied protein concentrations in the range of 2–55 $mg \cdot mL^{-1}$ that are injected into a 100 µL loop. SAXS frames were recorded every 1 s during elution and the first 50 files of the run were automatically selected and averaged by the data analysis pipeline *SmartMerge* of BM29 [30]. Sample frames were chosen according to peak regions in intensity, matching radius of gyration and high similarity using CORMAP [31]. If this automated data evaluation routine was not successful or overlapping species were merged, a manual data evaluation was performed using the software Scåtter of BIOISIS averaging frames in the region of a constant and stable R_g for each elution peak to analyse. The scattering intensities at different elution concentrations were compared and the highest measured concentration with best signal-to-noise ratio without detectable structure factor effects was used for further data analysis.

Further data analysis was performed using the software available within the ATSAS [32] and SCÅTTER software packages. Guinier analysis was performed in a q-range with qR_g <1.3 yielding the parameters R_g and I (0). The integrated scattering area of qI (q) versus q with upper limit of q_{max} = 0.2 was used for determining the correlation volume V_c defined as $I(0)/\int qI(q)dq$ yielding the parameter $Q_R = V_c^2/R_g$. The mass of a protein is then obtained as $M_m = Q_R/0.1231$ according to Rambo *et al.* [17]. The molecular weight was additionally calculated from the

Porod volume V_P as described by Petoukhov *et al.* [33], which was empirically shown to be proportional to the M_m with a factor of 0.625. Pair distribution functions $P(r)$ were calculated using the program DATGNOM. Theoretical scattering curves of the monomer and dimer were computed from the crystallographic structure 1DG3 and crystallographic dimer model (Fig. 1B) and fitted to the measured data using the program CRYSOL [34]. The excess scattering density of the hydration layer was used as a free fitting parameter resulting in dro = 0.06 for farn-hGBP1 in nucleotide-free solution (100% monomeric). Additionally, a constant background variable was left as floating parameter.

Structural modelling of the hGBP1 monomers and dimers was performed by rigid-body modelling using the software programs SASREF and EOM from the ATSAS package [35]. For SASREF and EOM calculations, rigid-bodies were extracted from the crystallographic protein structure 1DG3 of the full-length protein with the LG domain (aa 1–308 of 1DG3), MD domain (309–478), C12 helix (479–565) and C13 helix (566–583) as rigid-domains. To construct an atomic hGBP1 dimer model, the LG domains of GppNHp-bound full-length hGBP1 [23] (1F5N) were aligned to the GppNHp-bound dimeric crystal structure 2BC9 of the truncated LG domain construct [10]. For rigid-body modelling using SASREF, specific contact information was provided to ensure the connectivity of the separated domains and contact between the C13 α-helical domains for the hGBP1 dimer, which was described to be an additional dimer interface earlier [11]. Each condition was used for 10 SASREF runs to generate rigid-body models and the best model was chosen based on the smallest χ^2 and lowest accumulated penalty value. EOM modelling was performed using the rigid-body domains described above and the known amino acid sequences as input. Flexible linkers consisting of 10 amino acids were simulated by EOM as dummy beads that connect the rigid-body domains. Amino acids accounting for flexible linkers were deleted from the rigid-domains correspondingly. For EOM calculations, helices 12 and 13 were kept as found in the crystal structure. P2 symmetry conditions were used for hGBP1 dimer modelling. A pool of 10 000 different structural conformations was first generated by EOM that was subjected to the selection of the ensemble distribution. SAXS data and structural models are publicly available in the SASBDB [41].

Hydrodynamic calculations

The hydrodynamic properties were determined using both HYDROPRO [36] and SOLUTION MODELLER (SOMO) [37–39]. In general, we used the program JSCATTER for data fitting and analysis [40].

To obtain a structural dimer model, the monomer crystal structure of hGBP1 crystallized in the presence of GppNHp (1F5N) was duplicated and each one aligned to each of the LG domains that are crystallized as dimers in the presence of GppNHp (2BC9) using PyMOL to generate a hGBP1 dimer model ('1F5N-2BC9', see Fig. 1B).

For HYDROPRO calculations of all pdb structures, the calculated buffer viscosity using the ZETASIZER software, and the average partial specific volume as described in AUC methods are used. For Solution Modeller hydrodynamic calculations [37], SoMo overlap bead models are calculated and Zeno hydrodynamics algorithm is used to calculate the hydrodynamic parameters.

Acknowledgements

This work was supported by DFG grant STA 1325/2-1 to AMS. CL acknowledges the support of the International Helmholtz Research School of Biophysics and Soft Matter (BioSoft). This work is based upon experiments performed on the instruments BM29 at the European Synchrotron Radiation Facility (ESRF). We acknowledge the ESRF for provision of synchrotron radiation facilities and we thank Dr Martha Brennich for excellent assistance in using BM29. We also thank Prof Dr Dieter Willbold for providing access to the biochemistry labs of the ICS-6 institute. We thank Dr Gerrit Praefcke for provision of the plasmids coding for hGBP1 and farnesyltransferase subunits α/β. We also thank Dr. Ralf Biehl for provision of software tools used.

Conflict of interest

The authors declare no conflict of interest.

Author contributions

CL prepared samples for all measurements. SI, AC and RB-S provided expertise and equipment for protein expression and purification. CL planed all experiments and analysed all experimental data except AUC data. CL performed all measurements except AUC measurements. TZ and LN-S performed AUC measurements under the supervision of LN-S. CL, LN-S and AMS wrote the manuscript. AMS and CH provided funding for the project. AMS coordinated and supervised the project. All authors discussed the results and commented on the manuscript.

References

1 Wittinghofer A & Vetter IR (2011) Structure-function relationships of the G domain, a canonical switch motif. *Annu Rev Biochem* **80**, 943–971.
2 Gasper R, Meyer S, Gotthardt K, Sirajuddin M & Wittinghofer A (2009) It takes two to tango: regulation

of G proteins by dimerization. *Nat Rev Mol Cell Biol* **10**, 423–429.
3 Praefcke GJK & McMahon HT (2004) The dynamin superfamily: Universal membrane tubulation and fission molecules? *Nat Rev Mol Cell Biol* **5**, 133–147.
4 Mettlen M, Pucadyil T, Ramachandran R & Schmid SL (2009) Dissecting dynamin's role in clathrin-mediated endocytosis. *Biochem Soc Trans* **37**, 1022–1026.
5 Daumke O & Praefcke GJK (2016) Invited review: Mechanisms of GTP hydrolysis and conformational transitions in the dynamin superfamily. *Biopolymers* **105**, 580–593.
6 Prakash B, Praefcke GJ, Renault L, Wittinghofer A & Herrmann C (2000) Structure of human guanylate-binding protein 1 representing a unique class of GTP-binding proteins. *Nature* **403**, 567–571.
7 Britzen-Laurent N, Bauer M, Berton V, Fischer N, Syguda A, Reipschläger S, Naschberger E, Herrmann C & Stürzl M (2010) Intracellular trafficking of guanylate-binding proteins is regulated by heterodimerization in a hierarchical manner. *PLoS ONE* **5**, e14246.
8 Fres JM, Müller S & Praefcke GJK (2010) Purification of the CaaX-modified, dynamin-related large GTPase hGBP1 by coexpression with farnesyltransferase. *J Lipid Res* **51**, 2454–2459.
9 Praefcke GJK, Kloep S, Benscheid U, Lilie H, Prakash B & Herrmann C (2004) Identification of residues in the human guanylate-binding protein 1 critical for nucleotide binding and cooperative GTP hydrolysis. *J Mol Biol* **344**, 257–269.
10 Ghosh A, Praefcke GJK, Renault L, Wittinghofer A & Herrmann C (2006) How guanylate-binding proteins achieve assembly-stimulated processive cleavage of GTP to GMP. *Nature* **440**, 101–104.
11 Vöpel T, Hengstenberg CS, Peulen T-O, Ajaj Y, Seidel CAM, Herrmann C & Klare JP (2014) Triphosphate induced dimerization of human guanylate binding protein 1 involves association of the C-terminal helices: a joint double electron-electron resonance and FRET study. *Biochemistry* **53**, 4590–4600.
12 Shydlovskyi S, Zienert AY, Ince S, Dovengerds C, Hohendahl A, Dargazanli JM, Blum A, Günther SD, Kladt N, Stürzl M *et al.* (2017) Nucleotide-dependent farnesyl switch orchestrates polymerization and membrane binding of human guanylate-binding protein 1. *Proc Natl Acad Sci USA* **114**, E5559–E5568.
13 Vöpel T, Syguda A, Britzen-Laurent N, Kunzelmann S, Lüdemann M-B, Dovengerds C, Stürzl M & Herrmann C (2010) Mechanism of GTPase-activity-induced self-assembly of human guanylate binding protein 1. *J Mol Biol* **400**, 63–70.
14 Kunzelmann S, Praefcke GJK & Herrmann C (2006) Nucleotide binding and self-stimulated GTPase activity of human guanylate-binding protein 1 (hGBP1). *Methods Enzymol* **404**, 512–527.
15 Ince S, Kutsch M, Shydlovskyi S & Herrmann C (2017) The human guanylate-binding proteins hGBP-1 and hGBP-5 cycle between monomers and dimers only. *FEBS J* **284**, 2284–2301.
16 Durand D, Vivès C, Cannella D, Pérez J, Pebay-Peyroula E, Vachette P & Fieschi F (2010) NADPH oxidase activator p67phox behaves in solution as a multidomain protein with semi-flexible linkers. *J Struct Biol* **169**, 45–53.
17 Rambo RP & Tainer JA (2013) Accurate assessment of mass, models and resolution by small-angle scattering. *Nature* **496**, 477–481.
18 Tria G, Mertens HDT, Kachala M & Svergun DI (2015) Advanced ensemble modelling of flexible macromolecules using X-ray solution scattering. *IUCrJ* **2**, 207–217.
19 Vöpel T, Kunzelmann S & Herrmann C (2009) Nucleotide dependent cysteine reactivity of hGBP1 uncovers a domain movement during GTP hydrolysis. *FEBS Lett* **583**, 1923–1927.
20 Stadler AM, Knieps-Grünhagen E, Bocola M, Lohstroh W, Zamponi M & Krauss U (2016) Photoactivation reduces side-chain dynamics of a LOV photoreceptor. *Biophys J* **110**, 1064–1074.
21 Röllen K, Granzin J, Batra-safferling R & Stadler AM (2018) Small-angle X-ray scattering study of the kinetics of light-dark transition in a LOV protein. *PLoS ONE* **13**, 13–18.
22 Praefcke GJK, Geyer M, Schwemmle M, Robert Kalbitzer H & Herrmann C (1999) Nucleotide-binding characteristics of human guanylate-binding protein 1 (hGBP1) and identification of the third GTP-binding motif. *J Mol Biol* **292**, 321–332.
23 Prakash B, Renault L, Praefcke GJK, Herrmann C & Wittinghofer A (2002) Triphosphate structure of guanylate-binding protein 1 and implications for nucleotide binding and GTPase mechanism. *EMBO J* **19**, 4555–4564.
24 Laue T, Shah B, Ridgeway T & Pelletier S (1992) Computer aided interpretation of analytical sedimentation data for proteins. In Analytical ultracentrifuge in biochemistry and polymer science (Harding SE, Rowe AJ & Horton JC, eds), pp. 90–125. UK, Cambridge.
25 Schuck P (2000) Size-distribution analysis of macromolecules by sedimentation velocity ultracentrifugation and Lamm equation modeling. *Biophys J* **78**, 1606–1619.
26 Brown PH & Schuck P (2006) Macromolecular size-and-shape distributions by sedimentation velocity analytical ultracentrifugation. *Biophys J* **90**, 4651–4661.
27 Brown PH, Balbo A & Schuck P (2008) Characterizing protein-protein interactions by sedimentation velocity analytical ultracentrifugation. *Curr Protoc Immunol* 1–39.

28 Pernot P, Round A, Barrett R, De Maria Antolinos A, Gobbo A, Gordon E, Huet J, Kieffer J, Lentini M, Mattenet M *et al.* (2013) Upgraded ESRF BM29 beamline for SAXS on macromolecules in solution. *J Synchrotron Radiat* **20**, 660–664.
29 Brennich ME, Round AR & Hutin S (2017) Online size-exclusion and ion-exchange chromatography on a SAXS beamline. *J Vis Exp*, 1–9.
30 Brennich ME, Kieffer J, Bonamis G, De Maria Antolinos A, Hutin S, Pernot P & Round A (2016) Online data analysis at the ESRF bioSAXS beamline, BM29. *J Appl Crystallogr* **49**, 203–212.
31 De Maria Antolinos A, Pernot P, Brennich ME, Kieffer J, Bowler MW, Delageniere S, Ohlsson S, Malbet Monaco S, Ashton A, Franke D *et al.* (2015) ISPyB for BioSAXS, the gateway to user autonomy in solution scattering experiments. *Acta Crystallogr D* **71**, 76–85.
32 Konarev PV, Volkov VV, Sokolova AV, Koch MHJ & Svergun DI (2003) PRIMUS: A Windows PC-based system for small-angle scattering data analysis. *J Appl Crystallogr* **36**, 1277–1282.
33 Petoukhov MV, Franke D, Shkumatov AV, Tria G, Kikhney AG, Gajda M, Gorba C, Mertens HDT, Konarev PV & Svergun DI (2012) New developments in the ATSAS program package for small-angle scattering data analysis. *J Appl Crystallogr* **45**, 342–350.
34 Svergun DI, Barberato C & Koch MH (1995) CRYSOL – A program to evaluate X-ray solution scattering of biological macromolecules from atomic coordinates. *J Appl Crystallogr* **28**, 768–773.
35 Petoukhov MV & Svergun DI (2005) Global rigid body modeling of macromolecular complexes against small-angle scattering data. *Biophys J* **89**, 1237–1250.
36 de la Torre JG, Huertas ML & Carrasco B (2000) Calculation of hydrodynamic properties of globular proteins from their atomic-level structure. *Biophys J* **78**, 719–730.
37 Brookes E, Demeler B, Rosano C & Rocco M (2010) The implementation of SOMO (SOlution MOdeller) in the UltraScan analytical ultracentrifugation data analysis suite: enhanced capabilities allow the reliable hydrodynamic modeling of virtually any kind of biomacromolecule. *Europ Biophys J* **39**, 423–435.
38 Brookes E, Vachette P, Rocco M & Pérez J (2016) US-SOMO HPLC-SAXS module: dealing with capillary fouling and extraction of pure component patterns from poorly resolved SEC-SAXS data. *J Appl Crystallogr* **49**, 1827–1841.
39 Rocco M & Brookes E (2014) Dynamical aspects of biomacromolecular multi-resolution modelling using the UltraScan Solution Modeler (US-SOMO) Suite. In The Future of Dynamic Structural Science. NATO Science for Peace and Security Series A: Chemistry and Biology (Howard J, Sparkes H, Raithby P & Churakov A, eds), pp. 189–199. Springer, Dordrecht.
40 Biehl R (2018) Jscatter, a Program for Evaluation and Analysis of Experimental Data (Version 0.7.11). *Zenodo* https://doi.org/10.5281/zenodo.1470307.
41 Valentini E, Kikhney AG, Previtali G, Jeffries CM & Svergun DI (2015) SASBDB, a repository for biological small-angle scattering data. *Nucleic Acids Res* **43**, D357–D363.